THE JOURNAL OF PHYSICAL CHEMISTRY LETTERS
A JOURNAL OF THE AMERICAN CHEMICAL SOCIETY

pubs.acs.org/JPCL

Letter

Cost-Effective Digital Discovery of Aza-Hydrocarbons via Isomerization for Inverted Singlet−Triplet Emitters

Ramalingam Mahaan and Zhigang Shuai*

Cite This: *J. Phys. Chem. Lett.* 2026, 17, 6233−6244

Read Online

ACCESS | Metrics & More | Article Recommendations | Supporting Information

ABSTRACT: Hund's rule, derived from direct exchange (K), dictates that triplet (T_1) lies below singlet (S_1), leading to the 25% limit for electrofluorescence. Kinetic exchange ($-t^2/U$) from charge-transfer perturbation can stabilize S_1 over T_1, enabling inverted singlet−triplet (IST) gaps and offering a promising route to triplet harvesting. Such materials are exceedingly rare, and systematic design remains elusive. Here, we employ newly developed target-state optimized density functional theory (TSO-DFT) for cost-effective excited-state calculations, yielding reliable IST signatures with the B3LYP functional. Subsequently, we apply a high-throughput virtual screening (HTVS) to explore nitrogen-doped hydrocarbons derived from $C_{10}H_8$, $C_{14}H_{10}$, $C_{16}H_{10}$, $C_{18}H_{12}$, and $C_{20}H_{12}$ molecular cores via isomerization. This workflow screens 118 081 viable structures down to 34 potential candidates exhibiting negative S_1-T_1 gaps, an appreciable oscillator strength of ≥0.01, and fast RISC rates (~10^8 s^{-1}). This study provides a discovery pipeline for novel IST emitters and a curated library of visible-light candidates for next-generation optoelectronics.

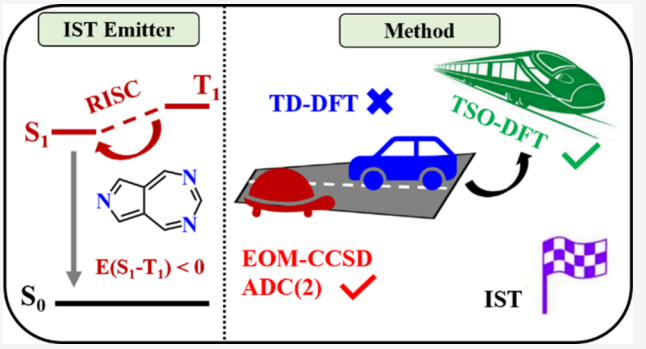

The spin multiplicity of excited states in molecules is crucial for organic electroluminescence.[1] This spin statistics limit the internal quantum efficiency (IQE) of organic light-emitting diodes (OLEDs) owing to the 1:3 singlet:triplet excited-state ratio and the spin-forbidden nature of triplet-state emission.[2] Considerable attention has been paid to optoelectronic emitters owing to their rich photophysical properties and versatile device applications, which are linked to the unique characteristics and evolution of their singlet and triplet excited states. To address this fundamental limitation, two primary strategies for harvesting photons from dark triplet excited states have been developed. The first approach employs transition metal complexes that introduce strong spin−orbit coupling (SOC), enabling triplet-state emission via phosphorescence.[3,4] The second strategy employs purely organic molecules that exhibit thermally activated delayed fluorescence (TADF). These materials are designed with a minimal energy separation between their S_1 and T_1 excited states. This small S_1-T_1 gap allows ambient thermal energy to promote triplet excitons back to singlets via reverse intersystem crossing (RISC).[5] While the TADF mechanism bypasses the use of costly transition metals, the resulting delayed fluorescence typically has a lifetime in the microsecond-to-millisecond range. This extended duration allows detrimental annihilation processes to compete effectively with the delayed fluorescence of the triplet excitons. Such annihilations contribute to a decrease in device efficiency at high operating currents, a phenomenon known as an efficiency roll-off in OLEDs. Furthermore, these processes can generate high-energy excitons that accelerate the chemical degradation of materials, which is a significant challenge in blue OLEDs.[6]

The discovery of negative S_1-T_1 gaps ($\Delta E_{ST} < 0$) has sparked a tremendous amount of interest, as it enables the natural conversion of electropumped triplets into singlet emission.[7] Such violations of Hund's rule were previously confined to unstable diradicals, to charge-transfer excited states in large molecules, and to systems exhibiting strong light−matter coupling.[8−11] A paradigm shift occurred with the theoretical identification of cyclazine compounds exhibiting negative ΔE_{ST} values, termed inverted singlet−triplet (IST) emitters (Figure 1a).[12] This unusual property offers novel avenues for improving device performance. A negative S_1-T_1 gap facilitates more efficient RISC and exciton utilization by enabling thermodynamically favorable downconversion without requiring thermal activation. The inversion of singlet−triplet state ordering arises from a delicate balance between direct exchange interactions and secondary superexchange energy, namely, $\Delta E_{ST} = -\frac{t^2}{\Delta E} + K$, where direct exchange

Received: March 31, 2026
Revised: May 5, 2026
Accepted: May 15, 2026
Published: May 20, 2026

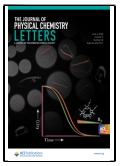

https://doi.org/10.1021/acs.jpclett.6c01031
J. Phys. Chem. Lett. 2026, 17, 6233−6244

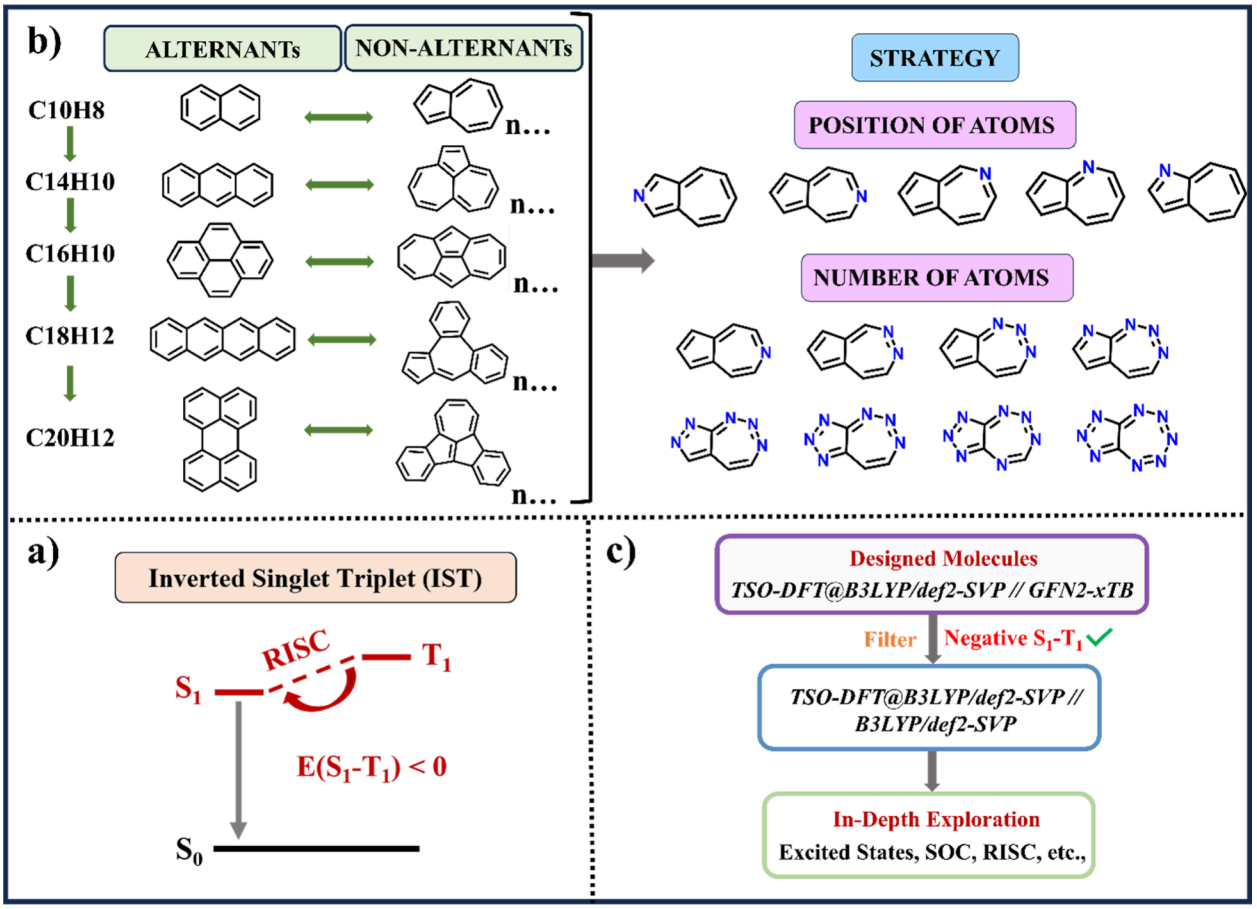

Figure 1. (a) Mechanism of inverted singlet−triplet (IST) emission. (b) Molecular building blocks and design strategies. (c) Computational screening workflow used in this study.

interaction K stabilizes the triplet state (Hund's rule) and the first term is the superexchange energy first discovered by P. W. Anderson, which is a secondary effect, usually small, but could be remarkable for a charge-transfer type of excited state, outweighing the direct exchange interaction, and producing a negative S_1-T_1 gap.[13,14] Although various azaphenalene analogues have been investigated experimentally since the 1980s for their photophysical properties and later as TADF emitters.[15,16] The four-decade gap between the identification of azaphenalenes as molecules with an inverted energy gap and their application in devices, even within the same molecular family, underscores the rarity of compounds that exhibit singlet−triplet inversion.[17]

Recent research has expanded the known examples of scarce IST materials that violate Hund's rule, and the underlying mechanisms remain an active area of investigation. Establishing new design principles for inverted gaps that depend on key factors to fine-tune control over electronic interactions is vital.[18] Excitation energies are commonly calculated using time-dependent density functional theory (TD-DFT), a workhorse of computational photophysics. Unfortunately, standard TD-DFT fails to predict the inverted gaps in IST compounds.[19] Consequently, all quantum chemistry methods based on a single-excitation framework, including configuration interaction singles (CIS) and TD-DFT (with or without the Tamm−Dancoff approximation), are fundamentally incapable of accurately describing these systems. While high-level methods such as multireference or coupled-cluster theory provide the necessary accuracy, their prohibitive computational cost limits their applicability to larger molecules.[20] A further complication is that in these anti-Hund molecules, in which the S_1 state typically has very low oscillator strengths (f), often the S_1-S_0 transition is symmetry-forbidden, rendering S_1 a nonemissive dark state.[21] Therefore, IST materials that combine a negative ΔE_{ST} with efficient light emission are exceptionally rare, and there are few clear design strategies. Motivated by the need for efficient high-throughput virtual screening (HTVS) of IST compounds, we explored whether simpler, cost-effective calculations could serve as a reliable prescreening tool, offering accuracy comparable to more expensive methods. Here, we utilize a new, practical, and accurate computational protocol to predict IST gaps. This protocol was subsequently employed to explore novel chemical motifs that function as highly emissive anti-Hund materials, thereby advancing this promising yet underexplored frontier of molecular design.

MATERIALS PERSPECTIVE

Initial work on closed-shell inherent IST molecules focused on cyclazine and its derivatives, later expanding to include nonalternant hydrocarbons.[22] In 2019, Ehrmaier et al. used time-resolved spectroscopy on a heptazine chromophore. They reported the surprising absence of delayed fluorescence, indicative of an exceptionally long S_1-state lifetime and the presence of an inverted S_1-T_1 gap.[23] In a significant high-throughput screening study, Aizawa et al. theoretically

https://doi.org/10.1021/acs.jpclett.6c01031
J. Phys. Chem. Lett. 2026, 17, 6233−6244

identified and subsequently synthesized heptazine derivative HzTFEX2 from 34 596 candidates. The compound exhibited an experimental ΔE_{ST} of −11 meV, a non-zero S_1 oscillator strength, and an EQE of approximately 17%, resulting in delayed fluorescence with a short time constant of 0.2 μs.[24] In 2024, Sun et al. demonstrated that modifying heptazine with various substituents effectively yields negative ΔE_{ST} values (as low as −0.362 eV) and enhanced oscillator strengths (up to 0.04). These designed emitters also exhibit a rapid RISC rate of 10^8 s^{-1} and emit light across a broad spectrum ranging from 339 to 716 nm.[25] Despite considerable efforts to tune the negative ΔE_{ST} and oscillator strength (f) in cyclazine cores for potential IST chromophores,[26−28] the fundamental challenge of achieving the high visible-light emissivity required for practical device fabrication persists. Efforts to control the singlet−triplet energies of nonalternant hydrocarbons have explored multiple avenues, such as Heilbronner substitution, double-bond delocalization, through-bond charge transfer, and the design of bridged derivatives.[29−32] Alternative chromophores that combine a negative ΔE_{ST} (<0) with high oscillator strength have yet to be explored, despite their potential to advance optoelectronic devices. We address this gap by presenting the systematic study of excited-state inversion in alternant and nonalternant hydrocarbons.

METHODOLOGICAL PERSPECTIVE

Direct measurement of ΔE_{ST} in IST materials is experimentally challenging because the transition is spin-forbidden, necessitating complementary theoretical studies. Nevertheless, theoretical methods also face a significant challenge in achieving chemically accurate predictions of excited-state energies in IST materials. The most widely used and economical method for predicting ΔE_{ST}, TD-DFT, fails to capture excited-state inversion as it inadequately accounts for distinct excited-state configurations. The consensus in the literature is that describing S_1/T_1-state inversion requires computationally intensive, correlated, wave function-based methods. For example, methods such as an equation-of-motion coupled cluster with single and double excitations (EOM-CCSD), linear-response second-order approximate coupled-cluster singles and doubles (LR-CC2), second-order algebraic diagrammatic construction (ADC(2)), along with their spin-scaled variants (SCS), and state-averaged complete-active-space self-consistent-field-based techniques, including SA-CASSCF, strongly contracted N-electron valence-state perturbation theory (SC-NEVPT2). Complete-active-space perturbation theory (CASPT2) is frequently employed to study IST emitters. These methods are favored because they incorporate the necessary electron correlation at a tractable computational cost for targeted studies.[19,21,30,33] The computational cost of such calculations, often several hours per molecule, precludes their use in automated screening of thousands of candidates. The Pariser−Parr−Pople (PPP) semiempirical method offers an ultrafast and robust screening tool for IST emitters, although its underlying approximations miss hits for certain compound classes.[34] The physical origin of singlet−triplet inversion has been traced to a delicate balance between direct exchange and kinetic exchange (superexchange) contributions.[11] The latter, arising from virtual hopping processes, preferentially stabilizes the singlet state and can, when sufficiently strong, overcome the direct exchange-driven triplet stabilization:

$$\Delta E_{ST} = -\frac{t^2}{\Delta E} + K$$

where t is the hopping integral between involved orbitals, ΔE denotes the energy difference between the paired and unpaired configurations, and K represents the direct exchange interaction. This kinetic exchange mechanism is expressed mathematically in wave function theory by including doubly excited configurations.[35] In practice, double-hybrid functionals achieve only mixed success because their correlation effects require a judicious and benchmarked choice for reliable modulation.[36−38] Building on these principles, Zhang et al. developed target-state optimized density functional theory (TSO-DFT), which enforces an orbital-subspace constraint to prevent variational collapse while allowing full orbital relaxation for the target excited configuration.[39] This approach excels precisely where conventional TD-DFT fails, charge-transfer states, making it ideally suited for investigating IST emitters. Here, we utilize TSO-DFT to resolve the debate over the sign of the S_1-T_1 gap and to establish its magnitude within the HTVS domain.

BENCHMARK STUDY

TSO-DFT can be classified as a ΔSCF method, yet it circumvents the persistent issue of variational collapse by design. It partitions molecular orbitals into distinct subspaces based on a target excited state, thereby avoiding collapse by construction through an orbital-subspace constraint. In contrast, recent studies have achieved IST gaps using ΔSCF by imposing constraints on orbital overlap with a target state during the SCF procedure.[36,40] To benchmark the performance of the TSO-DFT method, we selected two standard methods, EOM-CCSD and ADC(2), as references. These methods are well established in the literature on IST emitters and have been widely used to validate new methodologies. Initially, we tested TSO-DFT on five experimentally reported IST emitters (5AP, A6AP-Cz, HzTFEX2, HzTFEP2, and HzTFET2), along with one positive-gap molecule, HzPipX2.[24,41,42] TSO-DFT predicted a negative S_1-T_1 gap for all compounds except A6AP-Cz, and it also failed to reproduce the positive gap for the closely related HzPipX2 molecule (Figure S1). Figure S2 presents a benchmark comparison of experimental values with three DFT functionals (B3LYP, PBE0, and M06) using the TSO-DFT method for the S_1 energy, T_1 energy, and S_1-T_1 gap. Both B3LYP and PBE0 yielded results comparable to the experimental S_1 energy, T_1 energy, and S_1-T_1 gap, except for A6AP-Cz, whereas M06 showed larger deviations. Accordingly, we selected the B3LYP functional for all subsequent calculations. As these initial results were insufficient to conclusively assess accuracy, we expanded our benchmark set to include 10 theoretically proposed cyclazine-based (molecules 1−10) and 10 nonalternant-based (molecules 11−20) compounds. The molecular structures and calculated excitation properties are summarized in Table S1, and trends are shown in Figures S3a−d and S4a−d. Figure S5a−f presents correlation plots of S_1 energies, T_1 energies, and ΔE_{ST} values for molecules 1−10 against the EOM-CCSD and ADC(2) reference levels. Table S2 summarizes the mean absolute deviations (MAD), root-mean-square deviations (RMSD), and linear correlation coefficients (R^2) between TSO-DFT and the two reference methods. For the cyclazine compounds, TSO-DFT showed excellent agreement with both reference methods. The MAD

https://doi.org/10.1021/acs.jpclett.6c01031
J. Phys. Chem. Lett. 2026, 17, 6233−6244

for S_1 energies was 0.219 eV against EOM-CCSD and 0.100 eV against ADC(2), with R^2 values of 0.95 and 0.96, respectively. For T_1 energies, the MAD values were 0.183 eV (EOM-CCSD) and 0.148 eV (ADC(2)), with nearly perfect correlations (R^2 = 1.00 for both). The ΔE_{ST} MAD values were 0.086 eV (EOM-CCSD) and 0.124 eV (ADC(2)). Notably, TSO-DFT achieved 100% accuracy in predicting the sign of the S_1-T_1 gap compared to both reference methods. For the nonalternant hydrocarbon emitters, Figure S6a−d shows correlation plots for S_1 and T_1 energies, and Table S3 reports the corresponding metrics. The MAD for S_1 energies was 0.155 eV (EOM-CCSD) and 0.138 eV (ADC(2)), with R^2 values of 0.92 and 0.86, respectively. For T_1 energies, the MAD values were 0.162 eV (EOM-CCSD) and 0.154 eV (ADC(2)), with R^2 values of 0.98 and 0.96, respectively. The ΔE_{ST} MAD was 0.096 eV against EOM-CCSD and 0.169 eV against ADC(2). TSO-DFT aligned with EOM-CCSD for all molecules except molecule 12, whereas ADC(2) predicted all nonalternant molecules with a negative S_1-T_1 gap. These results establish TSO-DFT as an accurate and cost-effective method, providing a practical and reliable computational tool for the rational design of IST emitters.

MATERIAL DESIGN

Most prior investigations of alternant and nonalternant hydrocarbons have employed limited, case-specific molecular selections, and systematic coverage of chemical space remains rare, albeit with a few exceptions.[43] To address this, we implemented a database-curated approach using PubChem to assemble a structurally diverse library. We selected specific molecular formulas, $C_{10}H_8$, $C_{14}H_{10}$, $C_{16}H_{10}$, $C_{18}H_{12}$, and $C_{20}H_{12}$, to represent a series of increasing molecular size and π-conjugation length. This progression enables systematic coverage of the spectral region from shorter to longer wavelengths through controlled π-extension. For each formula, we queried PubChem to compile a comprehensive set of neutral, closed-shell hydrocarbon isomers derived from isomerization of the parent cores. Structures containing formal charges, radical character, or carbon atoms with sp or sp^3 hybridization (with very few exceptions) were excluded. This search yielded 7, 20, 30, 36, and 57 unique neutral scaffolds for the $C_{10}H_8$, $C_{14}H_{10}$, $C_{16}H_{10}$, $C_{18}H_{12}$, and $C_{20}H_{12}$ series, respectively, as shown in Figures S7−S10. To systematically explore the impact of nitrogen doping on hydrocarbon properties, termed aza-hydrocarbons, we employed two systematic strategies: (i) varying the position of the nitrogen atoms and (ii) varying the number of nitrogen atoms introduced (Figure 1b). The positional strategy involved enumerating all unique doping sites within each hydrocarbon scaffold to avoid duplicate structures. The numerical strategy involved generating all possible doping configurations for a given number of nitrogen atoms, starting with one nitrogen atom and progressing to the theoretical maximum defined by the number of hydrogen atoms in the parent molecular formula. This comprehensive enumeration ensures coverage of structures predicted to exhibit spatially disjointed frontier molecular orbitals (FMOs). This key geometric feature promotes kinetic exchange while enabling comprehensive sampling of the full configuration space of nitrogen doping patterns. The resulting combinatorial libraries comprised large, unique libraries of N-doped hydrocarbons: 1021 ($C_{10}H_8$), 12 092 ($C_{14}H_{10}$), 22 562 ($C_{16}H_{10}$), 112 892 ($C_{18}H_{12}$), and 187 175 ($C_{20}H_{12}$) distinct molecules. In total, this process yielded a data set of 335 742 unique N-doped hydrocarbon structures. The initial libraries for $C_{18}H_{12}$ and $C_{20}H_{12}$ were prohibitively large for high-throughput computational screening, containing 112 892 and 187 175 unique structures, respectively. To render the screening computationally feasible, a subset of 13 core units (see Figures S9 and S10) was selected from each library based on their smaller exchange integral. This selection process resulted in a refined library of 42 211 structures for $C_{18}H_{12}$ and 40 195 for $C_{20}H_{12}$. Combined with the other libraries, this afforded a final total of 118 081 unique aza-hydrocarbon structures for further study (Table 1).

Table 1. Number of Studied Molecules and Summary of Molecular Screening Results across Different Hydrocarbon Families[a]

		$-\Delta E_{ST}$		no. of potential molecules		
molecular formula	no. of studied molecules	GFN2-xTB	B3LYP	S_1	f	both
$C_{10}H_8$	1021	4	3	3	2	2
$C_{14}H_{10}$	12 092	187	113	21	28	11
$C_{16}H_{10}$	22 562	800	407	52	349	11
$C_{18}H_{12}$	42 211	715	495	70	124	4
$C_{20}H_{12}$	40 195	491	391	51	63	6
total	118 081	2197	1409	197	566	34

[a]Screening criteria: $\Delta E_{ST} < 0$, $S_1 \geq 1.70$ eV, and oscillator strength (f) ≥ 0.01. The molecular structures for the 34 potential molecules are depicted in Figure 5.

COMPUTATIONAL PIPELINE

The systematic identification of potential IST emitters from a library of 118 081 molecules necessitates a carefully designed computational pipeline. An exhaustive geometry optimization of all structures at the DFT level (e.g., B3LYP/def2-SVP) is prohibitively expensive despite being the standard for accurately computing excited-state energy gaps. To overcome this challenge, we implemented a multitiered strategy that balances computational efficiency with requisite accuracy, as illustrated in Figure 1c. First, to rapidly preoptimize geometries from the initial library and correct local strain, all structures were refined using the MMFF force field.[44] These preconditioned geometries were then optimized using the semiempirical GFN2-xTB method,[45] which has been shown to reproduce DFT-optimized geometries with high fidelity for conjugated organic molecules and to yield reliable trends in energy gaps.[34] These preoptimized geometries were used as input for high-throughput excited-state screening using the TSO-DFT method. This efficient approach enabled the rapid identification of candidate molecules with a target negative S_1-T_1 energy gap. To ensure that these candidates represent true minima and possess accurate electronic properties, a final validation step was performed. All molecules exhibiting negative S_1-T_1 gaps in the initial screen were reoptimized at the B3LYP/def2-SVP level of theory, and subsequent frequency analysis confirmed the absence of imaginary modes. Their excited states were subsequently re-evaluated using TSO-DFT calculations at the same level of theory. This two-tiered workflow, which leverages fast, semiempirical methods for initial screening and reserves costly DFT calculations for final validation, enables accurate, computa-

https://doi.org/10.1021/acs.jpclett.6c01031
J. Phys. Chem. Lett. 2026, 17, 6233−6244

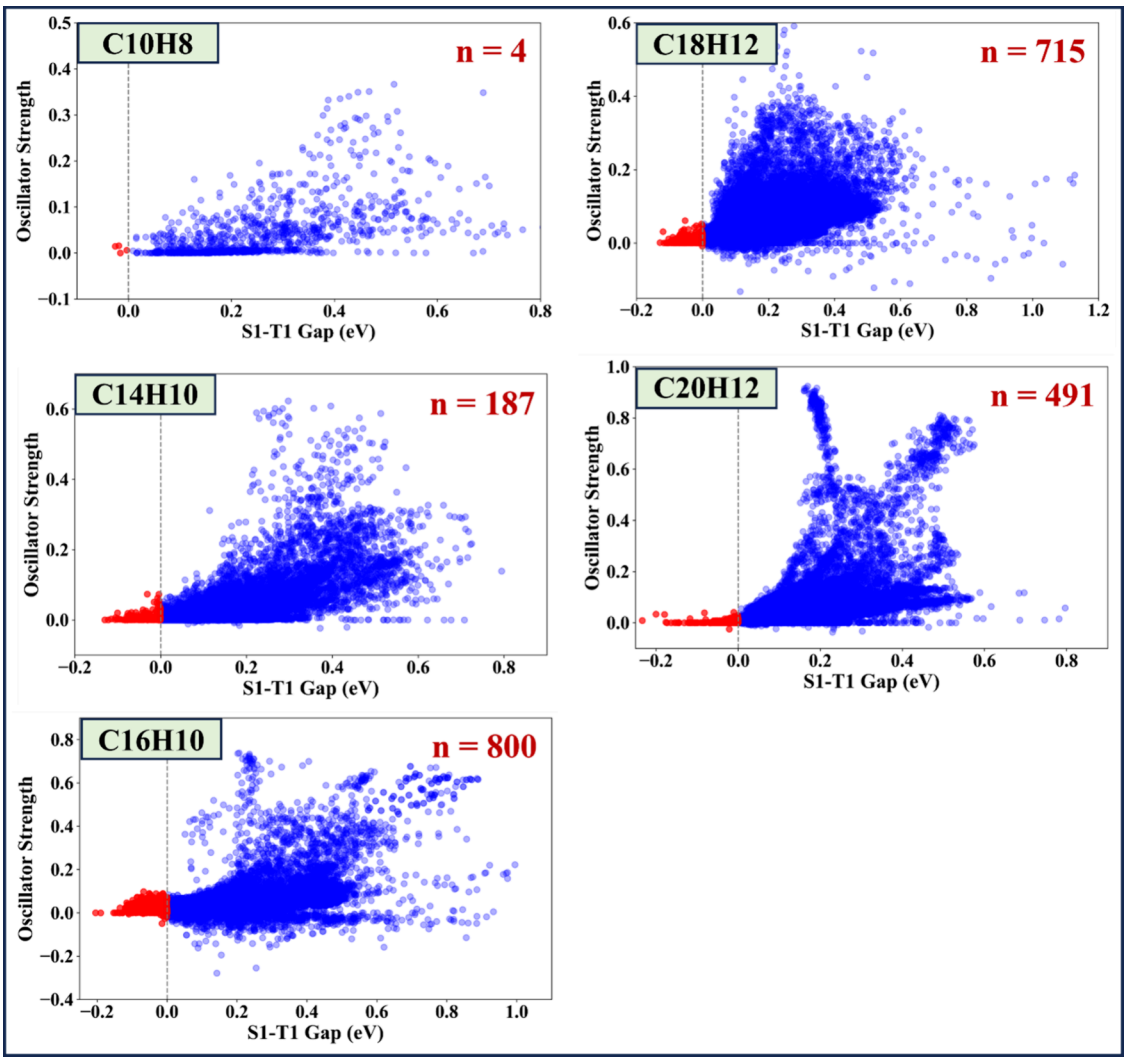

Figure 2. Relationship between the S_1-T_1 gap and oscillator strength across hydrocarbon families, calculated using GFN2-xTB-optimized geometries (red, negative ΔE_{ST}; blue, positive ΔE_{ST}; n = number of negative ΔE_{ST} candidates).

tionally tractable discovery of IST emitters across ultralarge chemical spaces.

■ ANALYSIS OF STRUCTURAL CLASSES

To evaluate the scalability, efficiency, and selectivity of our computational pipeline, we applied it to a systematically constructed series of five N-doped polycyclic hydrocarbon libraries. These libraries, based on the $C_{10}H_8$, $C_{14}H_{10}$, $C_{16}H_{10}$, $C_{18}H_{12}$, and $C_{20}H_{12}$ hydrocarbon cores, represent a combinatorial design space of 118 081 unique molecular structures. The initial stage of the pipeline involved rapid MMFF force-field optimization, followed by high-throughput geometry optimization of all designed structures using the semiempirical GFN2-xTB method. This step proved to be highly robust, with successful optimizations achieved across >99% of the total library. Subsequent calculation of excitation energies using the TSO-DFT method served as our primary filter for the target IST property ($\Delta E_{ST} < 0$). This high-throughput screening identified a primary candidate pool of 2197 molecules spread across all five libraries (Figure 2). The hit rate at this stage showed a clear dependency on molecular size and complexity, ranging from 0.4% for the smallest $C_{10}H_8$ library (4 of 1021) to 3.5% for the $C_{16}H_{10}$ library (800 of 22 562), suggesting that larger, more conjugated systems offer a greater configurational space for engineering the electronic conditions necessary for a negative S_1-T_1 gap. Figure 2 shows the statistics of the screened molecules as a function of the S_1-T_1 gap calculated by the TSO-DFT method. A well-known trade-off between the S_1-T_1 gap and f is evident in the plots, where f increases with the S_1-T_1 gap. Although balancing such trade-offs is a key concern, achieving excited-state control requires effort; thus, no single parameter can be optimized without sacrificing the others. As shown in Figure S11, the maximum vertical S_1 energies span ~5 eV for the $C_{10}H_8$ and $C_{14}H_{10}$ structures. This range decreases to ~3.50 eV for $C_{16}H_{10}$ and to ~3 eV for $C_{18}H_{12}$ and $C_{20}H_{12}$. These observations indicate that increasing molecular size and π-conjugation significantly shift the absorption to longer wavelengths. Furthermore, some compounds exhibit negative S_1 energies, indicating instability in the ground-state wave function, which may result from GFN2-xTB optimization. However, such instabilities are rare for molecules with a negative S_1-T_1 region, except in the case of $C_{16}H_{10}$ family.

The 2197 primary candidates were promoted to a rigorous DFT validation tier. Each structure was reoptimized at the B3LYP/def2-SVP level of theory, followed by TSO-DFT

https://doi.org/10.1021/acs.jpclett.6c01031
J. Phys. Chem. Lett. 2026, 17, 6233−6244

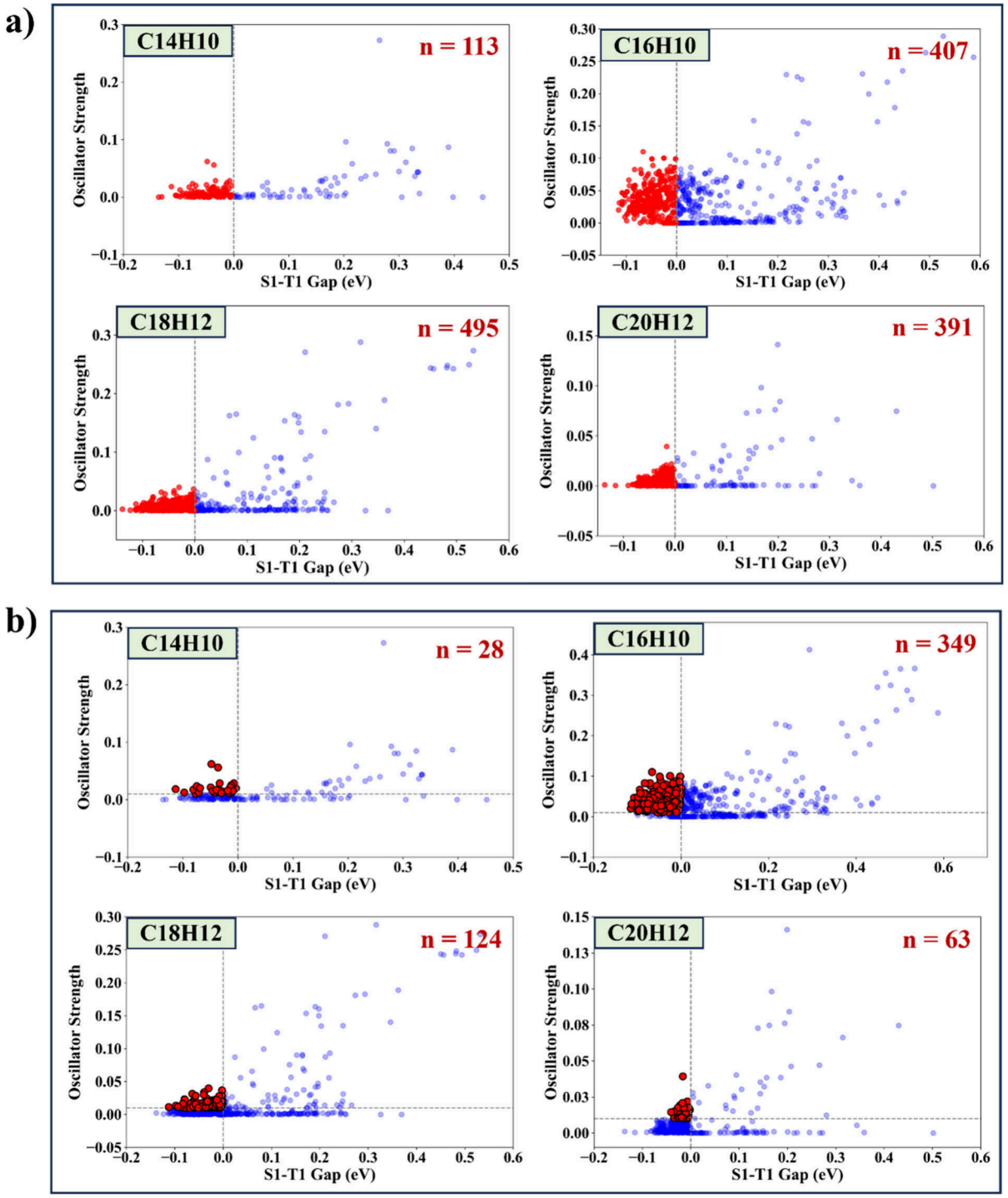

Figure 3. Relationship between the S_1-T_1 gap and oscillator strength across hydrocarbon families, calculated using B3LYP-optimized geometries (red, negative ΔE_{ST}; blue, positive ΔE_{ST}; n = number of negative ΔE_{ST} candidates) (a) without $f \geq 0.01$ and (b) with $f \geq 0.01$ criteria.

calculations to obtain refined excitation energies. This higher-fidelity validation is critical because it corrects for the semiempirical method's approximate nature and yields quantitatively reliable electronic structures. Of the initial 2197 GFN2-xTB hits, 1409 molecules retained a confirmed negative ΔE_{ST}, corresponding to an overall validation rate of 64% (Figure 3a). This substantial retention rate underscores the effectiveness of the GFN2-xTB method as a reliable prescreening tool for this specific electronic property, successfully filtering out most noncandidates while preserving the vast majority of true negatives for more costly DFT analysis. We now examine each category among the 1409 IST candidates. For each molecular family, we consider the number of negative-gap molecules derived from each bare core, the HOMO-LUMO exchange integral ($K_{H\text{-}L}$), and the frontier molecular orbitals of representative derivatives (Figures S12–S16). A clear correlation emerged across all molecular families. Hydrocarbon cores with low static $K_{H\text{-}L}$ values were markedly more likely to yield derivatives with a negative S_1-T_1 gap. This trend is illustrated by the productivity of specific parent cores

https://doi.org/10.1021/acs.jpclett.6c01031
J. Phys. Chem. Lett. 2026, 17, 6233−6244

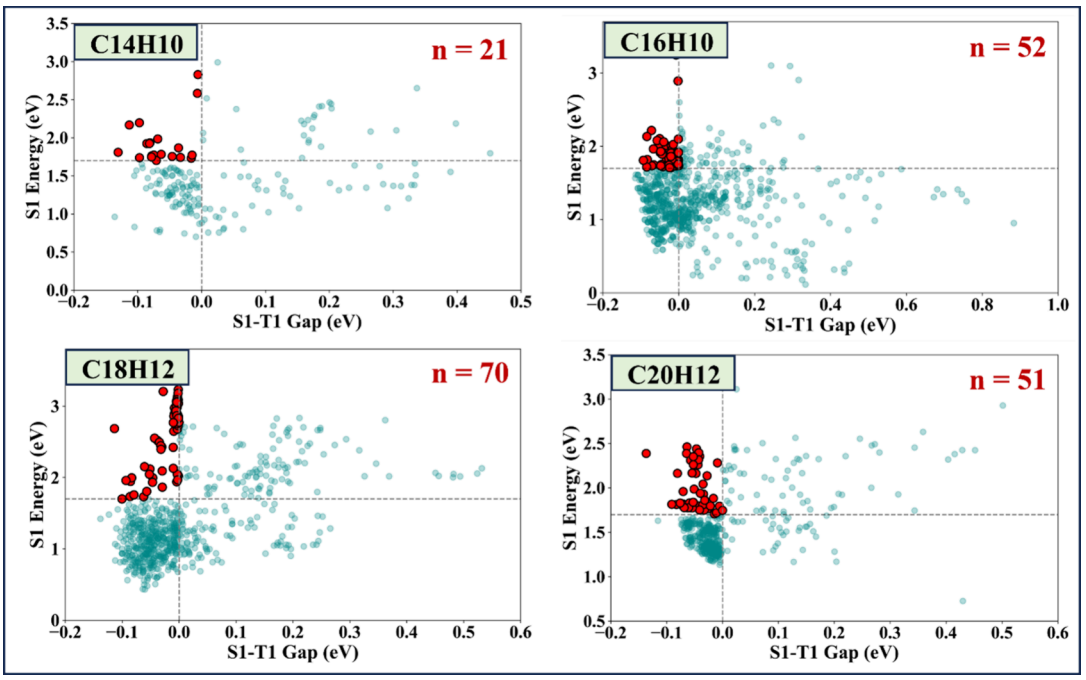

Figure 4. Relationship between the S_1-T_1 gap and S_1 energy across hydrocarbon families calculated using the B3LYP optimized geometries, where n is the number of negative ΔE_{ST} candidates with $S_1 \geq 1.70$ eV highlighted in red.

within each molecular family. For example, in the $C_{10}H_8$ family, the azulene core produced just two negative-gap derivatives (Figure S12a,b). Within the $C_{14}H_{10}$ family (Figure S13a−c), bare cores 3 and 13 generated 95 and 8 negative-gap derivatives, respectively. For the $C_{16}H_{10}$ family, bare cores 9, 20, and 22 yielded 25, 20, and 346 negative-gap derivatives, respectively (Figure S14a−c). This pattern of high output continues in larger families; in $C_{18}H_{12}$, bare core 16 produced 370 negative-gap derivatives (Figure S15a,b), and in $C_{20}H_{12}$, bare core 51 yielded 356 negative-gap derivatives (Figure S16a,b). Notably, more than half of the bare cores that yielded negative-gap derivatives among the 13 bare cores discussed here originated from the $C_{18}H_{12}$ and $C_{20}H_{12}$ families. While a small static exchange integral provides a favorable starting point, it is not determinative on its own. This is evident in instances in which bare cores with relatively high $K_{H\text{-}L}$ values nevertheless produced derivatives with negative gaps. For example, bare core 12 from the $C_{14}H_{10}$ family has a $K_{H\text{-}L}$ of 0.04 au, yet three of its derivatives, molecules 7344, 7361, and 7410, exhibit a diminished $K_{H\text{-}L}$ and a negative gap. Similar behavior was observed for bare cores 2, 4, 27, and 30 from the $C_{16}H_{10}$ family. These derivatives achieve inversion through structural modifications that enhance the kinetic exchange contribution, effectively overcoming an otherwise unfavorable direct exchange. These analyses establish $K_{H\text{-}L}$ as a key predictor, with values of ≤0.015 au (±0.005 au) representing an optimal regime for realizing a negative gap. Nevertheless, this HTVS study demonstrates that even cores with a high static exchange can be tuned toward inversion when structural variations sufficiently amplify the kinetic exchange contribution, ultimately yielding negative-gap emitters.

Having established a robust set of 1409 validated IST candidates, we first imposed a threshold on the oscillator strength ($f \geq 0.01$) to ensure that the S_1 state possesses sufficient radiative coupling for efficient fluorescence. This filter reduced the pool to 566 candidates (Figure 3b), showing that molecules with both a negative S_1-T_1 gap for efficient RISC and an appreciable oscillator strength are rare. Second, to target the relevant visible emitting region, we applied an S_1 energy threshold of 1.70 eV and yielded 197 molecules (Figure 4). The combined filter enforcing a negative S_1-T_1 gap, minimal oscillator strength, and sufficiently high S_1 energy produced a final set of 34 high-confidence candidates (Table 1 and Figure 5). They represent an extraordinary reduction of the original combinatorial space by a factor of nearly 3500 to 1. These final candidates are informatively distributed across all five hydrocarbon classes. Specifically, they originate from the following bare core structure numbers: 2 ($C_{10}H_8$), 3 and 12 ($C_{14}H_{10}$), 9 and 22 ($C_{16}H_{10}$), 16 ($C_{18}H_{12}$), and 17, 20, and 36 ($C_{20}H_{12}$). The systematic application of our pipeline across libraries spanning 2 orders of magnitude in size definitively establishes its efficacy and scalability. The workflow reliably navigates a vast combinatorial space through a tiered, property-specific filtering process, culminating in a very small, high-value set of molecules that simultaneously satisfy multiple demanding design criteria for IST emitters.

PROMISING IST CANDIDATES

The 34 candidates that passed the excitation screening filters ($\Delta E_{ST} < 0$ eV, $f \geq 0.01$, and $S_1 \geq 1.70$ eV) represent a high-confidence starting point. This final set comprises two molecules (azulene core) from the $C_{10}H_8$ family, 11 from the $C_{14}H_{10}$ family, 11 from the $C_{16}H_{10}$ family, four from the $C_{18}H_{12}$ family, and six from the $C_{20}H_{12}$ family, confirming the presence of viable IST emitters across all major structural classes studied. Table 2 summarizes the calculated excitation energies, SOC magnitudes, and RISC rates for these 34 candidates. The S_1-T_1 gaps range from −0.006 to −0.110 eV, magnitudes that are thermodynamically favorable for RISC. All molecules exhibit appreciable oscillator strengths (f = 0.01−0.110) for the S_1 state, indicating strong radiative decay channels necessary for efficient fluorescence. To quantitatively

https://doi.org/10.1021/acs.jpclett.6c01031
J. Phys. Chem. Lett. 2026, 17, 6233−6244

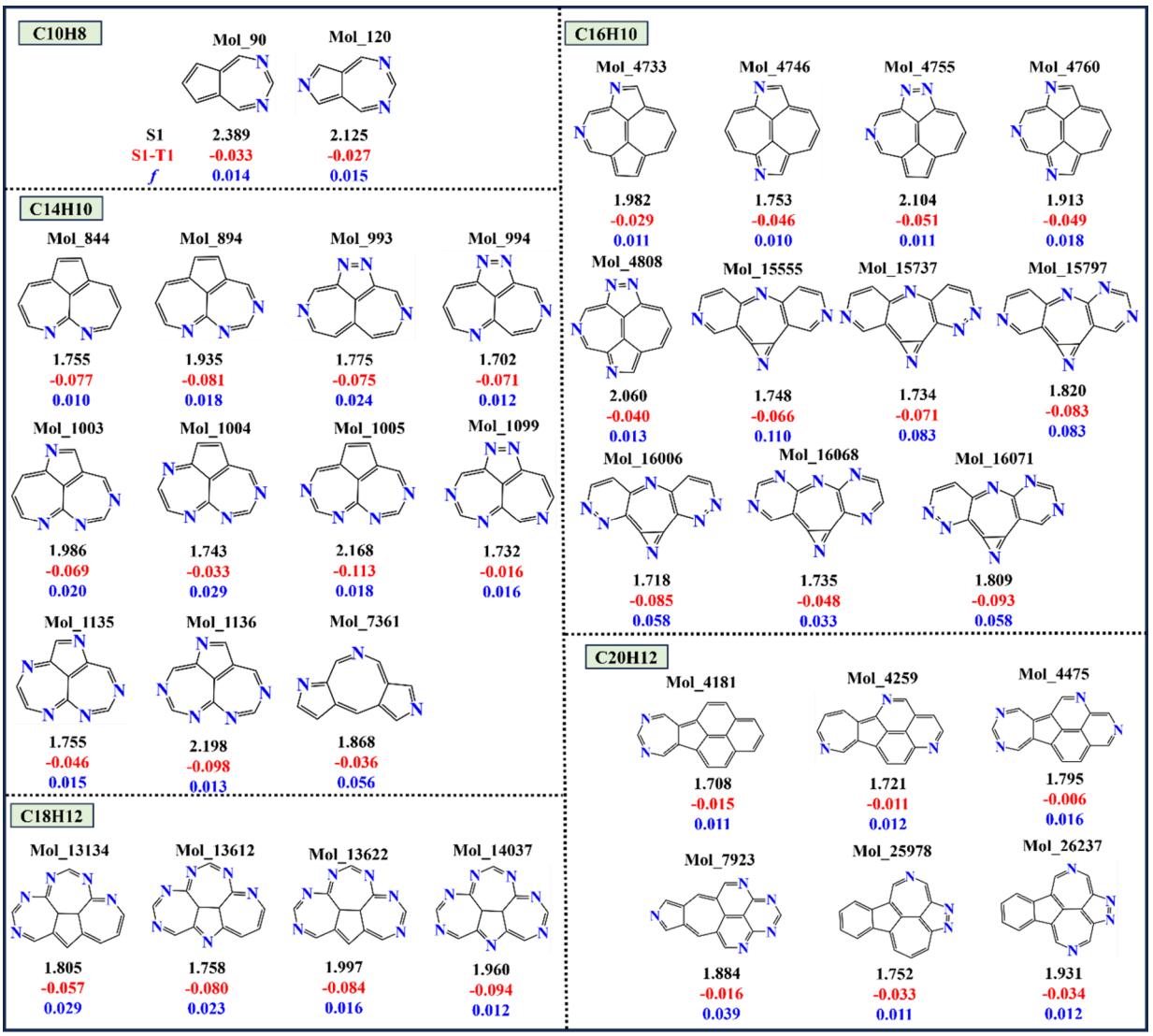

Figure 5. Final 34 potential IST candidates across different hydrocarbon families, with corresponding molecule ID, S_1 energy, S_1-T_1 gap, and oscillator strength (f) values.

evaluate IST emitter feasibility, we computed SOC matrix elements and RISC rates. The SOC between S_1 and T_1, together with the energy gap, governs the RISC process. The computed RISC rate, derived from the energy gaps and SOC matrix elements, is the most direct metric of TADF efficiency. Several candidates exhibit exceptionally high predicted RISC rates on the order of $\sim 10^7-10^8$ s^{-1}. These include molecule 90 from the $C_{10}H_8$ series; molecules 844, 894, 1003−1005, 1099, 1135, 1136, and 7361 from the $C_{14}H_{10}$ series; molecules 4733, 15 737, 16 068, and 16 071 from the $C_{16}H_{10}$ series; molecules 13 134, 13 612, 13 622, and 14 037 from the $C_{18}H_{12}$ series; and molecules 4181, 4259, 4475, and 7923 from the $C_{20}H_{12}$ series. These rates are comparable to or exceed those of the best-known TADF emitters, suggesting very fast triplet harvesting and high internal quantum efficiency. Among the 34 final candidates, 22 show strong potential as IST emitters, whereas the remaining molecules exhibit poor RISC due to weak SOC between the S_1 and T_1 states.

To conclude, we have presented a computationally efficient, scalable screening pipeline for discovering organic emitters with an inverted singlet−triplet energy gap. Our systematic investigation across the $C_{10}H_8$, $C_{14}H_{10}$, $C_{16}H_{10}$, $C_{18}H_{12}$, and $C_{20}H_{12}$ molecular series establishes clear structure−property relationships, enabling the targeted discovery of IST emitters with tunable emission profiles. Critically, the TSO-DFT methodology (with the B3LYP functional), benchmarked against experimentally reported and theoretically proposed IST molecules, shows superior accuracy in predicting negative ΔE_{ST} compared to standard EOM-CCSD and ADC(2) methods, establishing it as a uniquely cost-effective tool for IST emitter design. By integrating semiempirical prescreening with high-fidelity TSO-DFT validation, we successfully navigated a combinatorial space of more than 118 000 N-doped hydrocarbons, identifying candidates that simultaneously satisfy photophysical criteria: a negative ΔE_{ST}, visible range emission ($S_1 \geq 1.70$ eV), and oscillator strength ($f \geq 0.01$). The multistage screening reduces the candidate pool by nearly 4 orders of magnitude, ultimately isolating 34 potential IST molecules, several of which show promisingly high RISC rates of 10^7-10^8 s^{-1}. This result underscores the exceptional rarity of viable IST candidates within the vast combinatorial landscape of aza-hydrocarbons, where the kinetic exchange must be strong enough to overcome the intrinsic triplet preference, a search often likened to spotting a single spark in

https://doi.org/10.1021/acs.jpclett.6c01031
J. Phys. Chem. Lett. 2026, 17, 6233−6244

Table 2. Calculated Excitation Energies (in electronvolts), Oscillator Strengths (f), SOC Values (in inverse centimeters), and RISC Rates (in inverse seconds) for the Final 34 Potential IST Emitters

	energy				SOC			RISC
molecule id	S_1	T_1	S_1-T_1	f	S_1-T_1	S_1-T_2	S_1-T_3	T_1-S_1
				$C_{10}H_8$				
90	2.389	2.422	−0.033	0.014	1.243	0.000	0.067	4.25×10^8
120	2.125	2.152	−0.027	0.015	0.001	1.210	6.963	5.28×10^2
				$C_{14}H_{10}$				
844	1.755	1.832	−0.077	0.010	0.238	0.618	1.793	2.66×10^7
894	1.935	2.016	−0.081	0.018	0.491	0.617	1.245	1.18×10^8
993	1.775	1.850	−0.075	0.024	0.000	6.655	0.000	1.20×10
994	1.702	1.773	−0.071	0.012	0.073	4.823	0.183	2.35×10^6
1003	1.986	2.055	−0.069	0.020	0.303	0.459	6.628	4.01×10^7
1004	1.743	1.776	−0.033	0.029	0.371	1.370	6.251	3.79×10^7
1005	2.168	2.282	−0.113	0.018	0.927	3.170	0.911	5.23×10^8
1099	1.732	1.748	−0.016	0.016	0.566	5.666	2.496	6.69×10^7
1135	1.755	1.802	−0.046	0.015	0.649	7.092	0.457	1.39×10^8
1136	2.198	2.295	−0.098	0.013	0.955	1.209	6.723	5.09×10^8
7361	1.868	1.905	−0.036	0.056	2.181	1.211	1.203	1.37×10^9
				$C_{16}H_{10}$				
4733	1.982	2.010	−0.029	0.011	0.269	0.727	0.194	1.88×10^7
4746	1.753	1.799	−0.046	0.010	0.000	0.712	0.011	–
4755	2.104	2.154	−0.051	0.011	0.048	0.800	0.156	8.00×10^5
4760	1.913	1.961	−0.049	0.018	0.000	0.843	0.087	2.24×10^0
4808	2.060	2.100	−0.040	0.013	0.138	4.105	0.049	5.79×10^6
15 555	1.748	1.814	−0.066	0.110	0.000	0.201	12.667	1.10×10
15 737	1.734	1.805	−0.071	0.083	0.157	4.606	0.157	1.10×10^7
15 797	1.820	1.903	−0.083	0.083	0.073	0.190	9.397	2.62×10^6
16 006	1.718	1.803	−0.085	0.058	0.002	0.982	0.472	1.32×10^3
16 068	1.735	1.782	−0.048	0.033	0.516	0.379	5.026	9.04×10^7
16 071	1.809	1.902	−0.093	0.058	0.806	5.374	5.245	3.50×10^8
				$C_{18}H_{12}$				
13 134	1.805	1.862	−0.057	0.029	0.641	2.455	6.513	1.57×10^8
13 612	1.758	1.838	−0.080	0.023	0.386	6.586	7.324	7.23×10^7
13 622	1.997	2.081	−0.084	0.016	0.346	4.072	7.002	6.01×10^7
14 037	1.960	2.053	−0.094	0.012	0.335	8.249	8.918	6.10×10^7
				$C_{20}H_{12}$				
4181	1.708	1.722	−0.015	0.011	1.025	0.001	0.661	2.16×10^8
4259	1.721	1.733	−0.011	0.012	1.003	0.069	0.659	1.92×10^8
4475	1.795	1.801	−0.006	0.016	1.045	0.005	5.244	1.91×10^8
7923	1.884	1.900	−0.016	0.039	1.063	0.000	0.147	2.36×10^8
25 978	1.752	1.785	−0.033	0.011	0.013	0.700	0.021	4.93×10^4
26 237	1.931	1.965	−0.034	0.012	0.000	0.734	5.686	1.82×10^0

the darkness. Moreover, the explored chemical space itself suggests the existence of potential IST candidates with emission beyond 800 nm, pointing toward the promising yet underexplored near-infrared (NIR) region, an active area of research. Overall, this work establishes a robust computational framework and identifies high-potential molecular candidates to directly address the scarcity of next-generation organic IST emitters, paving the way for their future development of optoelectronic devices.

COMPUTATIONAL DETAILS

Ground-state geometry optimizations were performed using the B3LYP functional with ORCA version 6.0.1.[46,47] Excited-state EOM-CCSD and ADC(2) calculations were conducted using the Q-Chem software.[48] All TSO-DFT single-point calculations were performed using the Qbics 0.5 package with the B3LYP, PBE0, and M06 functionals.[49] Within the TSO-DFT framework, excitations were constructed based on simple single-electron excitations between the HOMO and LUMO orbitals.

The RISC rate between the T_1 and S_1 states was calculated using a semiclassical Marcus equation.[50,51]

$$k = \frac{|V|^2}{\hbar^2}\left(\frac{\pi}{\lambda k_B T}\right)^{1/2} \exp\left[-\frac{(\Delta G + \lambda)^2}{4\lambda k_B T}\right]$$

where k_B denotes the Boltzmann constant, T is the temperature (set to 300 K), and λ is the reorganization energy. A λ value of 0.15 eV was used, consistent with reported values that account for medium-induced relaxation effects.[52] SOC prefactor V was calculated at the optimized S_0 geometry using the PySOC code.[53] All calculations were carried out in the gas phase medium using the def2-SVP basis set.

ASSOCIATED CONTENT

Data Availability Statement

The data used to generate our results are available on GitHub (https://github.com/msmahaanr/High-Throughput-Virtual-Screening-of-Aza-Hydrocarbons-for-Inverted-Singlet-Triplet-Emitters.git).

https://doi.org/10.1021/acs.jpclett.6c01031
J. Phys. Chem. Lett. 2026, 17, 6233−6244

Supporting Information

The Supporting Information is available free of charge at https://pubs.acs.org/doi/10.1021/acs.jpclett.6c01031.

Excitation energies of reference IST emitters; benchmark results for cyclazine and nonalternant compounds; correlation plots of excitation energies and corresponding metrics; core hydrocarbon structures of $C_{10}H_8$, $C_{14}H_{10}$, $C_{16}H_{10}$, $C_{18}H_{12}$, and $C_{20}H_{12}$ families; diagram of the relationship between the S_1-T_1 gap and S_1 energy calculated using the GFN2-xTB optimized geometries; and calculated exchange integrals and their frontier molecular orbitals across all hydrocarbon families (PDF)

AUTHOR INFORMATION

Corresponding Author

Zhigang Shuai − *Guangdong Basic Research Center of Excellence for Aggregate Science, School of Science and Engineering, The Chinese University of Hong Kong, Shenzhen, Guangdong 518172, P. R. China; MOE Key Laboratory for Organic Optoelectronics and Molecular Engineering, Department of Chemistry, Tsinghua University, Beijing 100084, P. R. China;* orcid.org/0000-0003-3867-2331; Email: shuaizhigang@cuhk.edu.cn

Author

Ramalingam Mahaan − *Guangdong Basic Research Center of Excellence for Aggregate Science, School of Science and Engineering, The Chinese University of Hong Kong, Shenzhen, Guangdong 518172, P. R. China;* orcid.org/0000-0002-7722-3515

Complete contact information is available at: https://pubs.acs.org/10.1021/acs.jpclett.6c01031

Notes

The authors declare no competing financial interest.

ACKNOWLEDGMENTS

The authors are grateful to Dr. Jun Zhang and Prof. Jiali Gao for the help in using TSO-DFT.[39,49] This work is supported by the National Natural Science Foundation of China (Grants T2350009 and 22433007), the Guangdong Provincial Natural Science Foundation (Grant 2024A1515011185), and the Shenzhen City Peacock Team Project (Grant KQTD20240729102028011). R.M. and Z.S. are supported by the Guangdong Basic Research Center of Excellence for Aggregate Science. The computing exercise in this work was conducted on the High-Performance Computing Portal, which is under the administration of the Information Technology Services Office (ITSO) at the Chinese University of Hong Kong, Shenzhen.

REFERENCES

(1) Baldo, M. A.; O'Brien, D. F.; You, Y.; Shoustikov, A.; Sibley, S.; Thompson, M. E.; Forrest, S. R. Highly Efficient Phosphorescent Emission from Organic Electroluminescent Devices. *Nature* **1998**, *395* (6698), 151−154.

(2) Baldo, M. A.; Lamansky, S.; Burrows, P. E.; Thompson, M. E.; Forrest, S. R. Very High-Efficiency Green Organic Light-Emitting Devices Based on Electrophosphorescence. *Appl. Phys. Lett.* **1999**, *75* (1), 4−6.

(3) Yook, K. S.; Lee, J. Y. Organic Materials for Deep Blue Phosphorescent Organic Light-Emitting Diodes. *Adv. Mater.* **2012**, *24* (24), 3169−3190.

(4) Lee, J.; Chen, H.-F.; Batagoda, T.; Coburn, C.; Djurovich, P. I.; Thompson, M. E.; Forrest, S. R. Deep Blue Phosphorescent Organic Light-Emitting Diodes with Very High Brightness and Efficiency. *Nat. Mater.* **2016**, *15* (1), 92−98.

(5) Zysman-Colman, E., Reineke, S., Xie, G., Adachi, C., Eds. *Recent Advances in Thermally Activated Delayed Fluorescence Materials*; Frontiers Media SA, 2021.

(6) Dos Santos, J. M.; Hall, D.; Basumatary, B.; Bryden, M.; Chen, D.; Choudhary, P.; Comerford, T.; Crovini, E.; Danos, A.; De, J.; Diesing, S.; Fatahi, M.; Griffin, M.; Gupta, A. K.; Hafeez, H.; Hämmerling, L.; Hanover, E.; Haug, J.; Heil, T.; Karthik, D.; Kumar, S.; Lee, O.; Li, H.; Lucas, F.; Mackenzie, C. F. R.; Mariko, A.; Matulaitis, T.; Millward, F.; Olivier, Y.; Qi, Q.; Samuel, I. D. W.; Sharma, N.; Si, C.; Spierling, L.; Sudhakar, P.; Sun, D.; Tankelevičiūtė, E.; Duarte Tonet, M.; Wang, J.; Wang, T.; Wu, S.; Xu, Y.; Zhang, L.; Zysman-Colman, E. The Golden Age of Thermally Activated Delayed Fluorescence Materials: Design and Exploitation. *Chem. Rev.* **2024**, *124* (24), 13736−14110.

(7) Leupin, W.; Wirz, J. Low-Lying Electronically Excited States of Cycl[3.3.3]Azine, a Bridged 12.Pi.-Perimeter. *J. Am. Chem. Soc.* **1980**, *102* (19), 6068−6075.

(8) Dougherty, D. A. Spin Control in Organic Molecules. *Acc. Chem. Res.* **1991**, *24* (3), 88−94.

(9) Borden, W. T.; Iwamura, H.; Berson, J. A. Violations of Hund's Rule in Non-Kekule Hydrocarbons: Theoretical Prediction and Experimental Verification. *Acc. Chem. Res.* **1994**, *27* (4), 109−116.

(10) Segal, M.; Singh, M.; Rivoire, K.; Difley, S.; Van Voorhis, T.; Baldo, M. A. Extrafluorescent Electroluminescence in Organic Light-Emitting Devices. *Nat. Mater.* **2007**, *6* (5), 374−378.

(11) Difley, S.; Beljonne, D.; Van Voorhis, T. On the Singlet−Triplet Splitting of Geminate Electron−Hole Pairs in Organic Semiconductors. *J. Am. Chem. Soc.* **2008**, *130* (11), 3420−3427.

(12) Wrigley, L.; Schlenker, C. W. Singlet-Triplet Inversion. *Annu. Rev. Phys. Chem.* **2025**, *76* (1), 329−355.

(13) Won, T.; Nakayama, K.; Aizawa, N. Inverted Singlet−Triplet Emitters for Organic Light-Emitting Diodes. *Chem. Phys. Rev.* **2023**, *4* (2), 021310 DOI: 10.1063/5.0152834.

(14) Anderson, P. W. New Approach to the Theory of Superexchange Interactions. *Phys. Rev.* **1959**, *115* (1), 2−13.

(15) Leupin, W.; Magde, D.; Persy, G.; Wirz, J. 1,4,7-Triazacycl-[3.3.3]Azine: Basicity, Photoelectron Spectrum, Photophysical Properties. *J. Am. Chem. Soc.* **1986**, *108* (1), 17−22.

(16) Leupin, W.; Wirz, J. Low-Lying Electronically Excited States of Cycl[3.3.3]Azine, a Bridged 12.Pi.-Perimeter. *J. Am. Chem. Soc.* **1980**, *102* (19), 6068−6075.

(17) Audebert, P.; Kroke, E.; Posern, C.; Lee, S.-H. State of the Art in the Preparation and Properties of Molecular Monomeric *s* -Heptazines: Syntheses, Characteristics, and Functional Applications. *Chem. Rev.* **2021**, *121* (4), 2515−2544.

(18) Sandoval-Salinas, M. E.; Ricci, G.; Pérez-Jiménez, A. J.; Casanova, D.; Olivier, Y.; Sancho-García, J. C. Correlation *vs.* Exchange Competition Drives the Singlet−Triplet Excited-State Inversion in Non-Alternant Hydrocarbons. *Phys. Chem. Chem. Phys.* **2023**, *25* (39), 26417−26428.

(19) Loos, P.-F.; Lipparini, F.; Jacquemin, D. Heptazine, Cyclazine, and Related Compounds: Chemically-Accurate Estimates of the Inverted Singlet−Triplet Gap. *J. Phys. Chem. Lett.* **2023**, *14* (49), 11069−11075.

(20) Ricci, G.; San-Fabián, E.; Olivier, Y.; Sancho-García, J. C. Singlet-Triplet Excited-State Inversion in Heptazine and Related Molecules: Assessment of TD-DFT and *Ab Initio* Methods. *ChemPhysChem* **2021**, *22* (6), 553−560.

(21) Ricci, G.; Sancho-García, J.-C.; Olivier, Y. Establishing Design Strategies for Emissive Materials with an Inverted Singlet−Triplet Energy Gap (INVEST): A Computational Perspective on How

Symmetry Rules the Interplay between Triplet Harvesting and Light Emission. *J. Mater. Chem. C Mater.* **2022**, *10* (35), 12680−12698.
(22) Anwer, M.; Yin, S. Recent Progress and Prospects of Inverted Singlet-Triplet Energy Gap (INVEST) Materials in OLEDs. *Org. Electron.* **2025**, *144*, No. 107282.
(23) Ehrmaier, J.; Rabe, E. J.; Pristash, S. R.; Corp, K. L.; Schlenker, C. W.; Sobolewski, A. L.; Domcke, W. Singlet−Triplet Inversion in Heptazine and in Polymeric Carbon Nitrides. *J. Phys. Chem. A* **2019**, *123* (38), 8099−8108.
(24) Aizawa, N.; Pu, Y.-J.; Harabuchi, Y.; Nihonyanagi, A.; Ibuka, R.; Inuzuka, H.; Dhara, B.; Koyama, Y.; Nakayama, K.; Maeda, S.; Araoka, F.; Miyajima, D. Delayed Fluorescence from Inverted Singlet and Triplet Excited States. *Nature* **2022**, *609* (7927), 502−506.
(25) Sun, C.; Guo, Z.; Tang, Y.; Lu, X.; Lv, Q.; Li, P.; Zheng, C.; Chen, R. Design of Anti-Hund Organic Emitters Based on Heptazine. *ACS Appl. Mater. Interfaces* **2024**, *16* (44), 60648−60657.
(26) Anwer, M.; Yin, S. Symmetry-Breaking Strategy for Enhanced Oscillator Strength in Inverted Singlet−Triplet (INVEST) Emitters for OLED Applications. *Phys. Chem. Chem. Phys.* **2025**, *27* (45), 24545−24557.
(27) Bräse, S.; Hatakeyama, T.; Yasuda, T.; Zysman-Colman, E. Multi-Resonant Thermally Activated Delayed Fluorescence and Inverted Singlet-Triplet Energy Gap Materials. *Adv. Opt. Mater.* **2025**, *13* (23), e01830 DOI: 10.1002/adom.202501830.
(28) Dubbini, M.; Bonvini, F.; Savi, L.; Di Maiolo, F. Turning on Organic Radical Emitters. *J. Phys. Chem. C* **2024**, *128* (43), 18158−18169.
(29) Blaskovits, J. T.; Corminboeuf, C.; Garner, M. H. Singlet−Triplet Inversions in Through-Bond Charge-Transfer States. *J. Phys. Chem. Lett.* **2024**, *15* (40), 10062−10067.
(30) Terence Blaskovits, J.; Garner, M. H.; Corminboeuf, C. Symmetry-Induced Singlet-Triplet Inversions in Non-Alternant Hydrocarbons. *Angew. Chem., Int. Ed.* **2023**, *62* (15), e202218156 DOI: 10.1002/anie.202218156.
(31) Garner, M. H.; Blaskovits, J. T.; Corminboeuf, C. Enhanced Inverted Singlet−Triplet Gaps in Azaphenalenes and Non-Alternant Hydrocarbons. *Chem. Commun.* **2024**, *60* (15), 2070−2073.
(32) Garner, M. H.; Blaskovits, J. T.; Corminboeuf, C. Double-Bond Delocalization in Non-Alternant Hydrocarbons Induces Inverted Singlet−Triplet Gaps. *Chem. Sci.* **2023**, *14* (38), 10458−10466.
(33) Rivera Blair, L.; Nematiaram, T. Inverting Singlet−Triplet Gaps by Design. *J. Mater. Chem. C Mater.* **2025**, *13* (34), 17769−17779.
(34) Jorner, K.; Pollice, R.; Lavigne, C.; Aspuru-Guzik, A. Ultrafast Computational Screening of Molecules with Inverted Singlet−Triplet Energy Gaps Using the Pariser−Parr−Pople Semiempirical Quantum Chemistry Method. *J. Phys. Chem. A* **2024**, *128* (12), 2445−2456.
(35) de Silva, P. Inverted Singlet−Triplet Gaps and Their Relevance to Thermally Activated Delayed Fluorescence. *J. Phys. Chem. Lett.* **2019**, *10* (18), 5674−5679.
(36) Ghosh, S.; Bhattacharyya, K. Origin of the Failure of Density Functional Theories in Predicting Inverted Singlet−Triplet Gaps. *J. Phys. Chem. A* **2022**, *126* (8), 1378−1385.
(37) Maiz-Pastor, P.; Pérez-Jiménez, A. J.; Sancho-García, J. C. Double-Hybrid Density Functionals Applied to a Large Set of INVEST Systems: Validating the (SOS1-)PBE-DH-INVEST Expressions. *J. Mater. Chem. C Mater.* **2025**, *13* (28), 14211−14223.
(38) Sancho-García, J. C.; Brémond, E.; Ricci, G.; Pérez-Jiménez, A. J.; Olivier, Y.; Adamo, C. Violation of Hund's Rule in Molecules: Predicting the Excited-State Energy Inversion by TD-DFT with Double-Hybrid Methods. *J. Chem. Phys.* **2022**, *156* (3), 034105 DOI: 10.1063/5.0076545.
(39) Zhang, J.; Tang, Z.; Zhang, X.; Zhu, H.; Zhao, R.; Lu, Y.; Gao, J. Target State Optimized Density Functional Theory for Electronic Excited and Diabatic States. *J. Chem. Theory Comput.* **2023**, *19* (6), 1777−1789.
(40) Kunze, L.; Froitzheim, T.; Hansen, A.; Grimme, S.; Mewes, J.-M. ΔDFT Predicts Inverted Singlet−Triplet Gaps with Chemical Accuracy at a Fraction of the Cost of Wave Function-Based Approaches. *J. Phys. Chem. Lett.* **2024**, *15* (31), 8065−8077.
(41) Okumura, R.; Tanaka, H.; Shizu, K.; Fukushima, S.; Yasuda, Y.; Kaji, H. Development of an Organic Emitter Exhibiting Reverse Intersystem Crossing Faster than Intersystem Crossing. *Angew. Chem., Int. Ed.* **2024**, *63* (35), e202409670 DOI: 10.1002/anie.202409670.
(42) Wilson, K. D.; Styers, W. H.; Wood, S. A.; Woods, R. C.; McMahon, R. J.; Liu, Z.; Yang, Y.; Garand, E. Spectroscopic Quantification of the Inverted Singlet−Triplet Gap in Pentaazaphenalene. *J. Am. Chem. Soc.* **2024**, *146* (23), 15688−15692.
(43) Pollice, R.; Ding, B.; Aspuru-Guzik, A. Rational Design of Organic Molecules with Inverted Gaps between the First Excited Singlet and Triplet. *Matter* **2024**, *7* (3), 1161−1186.
(44) Halgren, T. A. Merck Molecular Force Field. I. Basis, Form, Scope, Parameterization, and Performance of MMFF94. *J. Comput. Chem.* **1996**, *17* (5−6), 490−519.
(45) Bannwarth, C.; Ehlert, S.; Grimme, S. GFN2-XTB—An Accurate and Broadly Parametrized Self-Consistent Tight-Binding Quantum Chemical Method with Multipole Electrostatics and Density-Dependent Dispersion Contributions. *J. Chem. Theory Comput.* **2019**, *15* (3), 1652−1671.
(46) Tirado-Rives, J.; Jorgensen, W. L. Performance of B3LYP Density Functional Methods for a Large Set of Organic Molecules. *J. Chem. Theory Comput.* **2008**, *4* (2), 297−306.
(47) Neese, F. The ORCA Program System. *WIREs Computational Molecular Science* **2012**, *2* (1), 73−78.
(48) Shao, Y.; Gan, Z.; Epifanovsky, E.; Gilbert, A. T. B.; Wormit, M.; Kussmann, J.; Lange, A. W.; Behn, A.; Deng, J.; Feng, X.; Ghosh, D.; Goldey, M.; Horn, P. R.; Jacobson, L. D.; Kaliman, I.; Khaliullin, R. Z.; Kuś, T.; Landau, A.; Liu, J.; Proynov, E. I.; Rhee, Y. M.; Richard, R. M.; Rohrdanz, M. A.; Steele, R. P.; Sundstrom, E. J.; Woodcock, H. L.; Zimmerman, P. M.; Zuev, D.; Albrecht, B.; Alguire, E.; Austin, B.; Beran, G. J. O.; Bernard, Y. A.; Berquist, E.; Brandhorst, K.; Bravaya, K. B.; Brown, S. T.; Casanova, D.; Chang, C.-M.; Chen, Y.; Chien, S. H.; Closser, K. D.; Crittenden, D. L.; Diedenhofen, M.; DiStasio, R. A.; Do, H.; Dutoi, A. D.; Edgar, R. G.; Fatehi, S.; Fusti-Molnar, L.; Ghysels, A.; Golubeva-Zadorozhnaya, A.; Gomes, J.; Hanson-Heine, M. W. D.; Harbach, P. H. P.; Hauser, A. W.; Hohenstein, E. G.; Holden, Z. C.; Jagau, T.-C.; Ji, H.; Kaduk, B.; Khistyaev, K.; Kim, J.; Kim, J.; King, R. A.; Klunzinger, P.; Kosenkov, D.; Kowalczyk, T.; Krauter, C. M.; Lao, K. U.; Laurent, A. D.; Lawler, K. V.; Levchenko, S. V.; Lin, C. Y.; Liu, F.; Livshits, E.; Lochan, R. C.; Luenser, A.; Manohar, P.; Manzer, S. F.; Mao, S.-P.; Mardirossian, N.; Marenich, A. V.; Maurer, S. A.; Mayhall, N. J.; Neuscamman, E.; Oana, C. M.; Olivares-Amaya, R.; O'Neill, D. P.; Parkhill, J. A.; Perrine, T. M.; Peverati, R.; Prociuk, A.; Rehn, D. R.; Rosta, E.; Russ, N. J.; Sharada, S. M.; Sharma, S.; Small, D. W.; Sodt, A.; Stein, T.; Stück, D.; Su, Y.-C.; Thom, A. J. W.; Tsuchimochi, T.; Vanovschi, V.; Vogt, L.; Vydrov, O.; Wang, T.; Watson, M. A.; Wenzel, J.; White, A.; Williams, C. F.; Yang, J.; Yeganeh, S.; Yost, S. R.; You, Z.-Q.; Zhang, I. Y.; Zhang, X.; Zhao, Y.; Brooks, B. R.; Chan, G. K. L.; Chipman, D. M.; Cramer, C. J.; Goddard, W. A.; Gordon, M. S.; Hehre, W. J.; Klamt, A.; Schaefer, H. F.; Schmidt, M. W.; Sherrill, C. D.; Truhlar, D. G.; Warshel, A.; Xu, X.; Aspuru-Guzik, A.; Baer, R.; Bell, A. T.; Besley, N. A.; Chai, J.-D.; Dreuw, A.; Dunietz, B. D.; Furlani, T. R.; Gwaltney, S. R.; Hsu, C.-P.; Jung, Y.; Kong, J.; Lambrecht, D. S.; Liang, W.; Ochsenfeld, C.; Rassolov, V. A.; Slipchenko, L. V.; Subotnik, J. E.; Van Voorhis, T.; Herbert, J. M.; Krylov, A. I.; Gill, P. M. W.; Head-Gordon, M. Advances in Molecular Quantum Chemistry Contained in the Q-Chem 4 Program Package. *Mol. Phys.* **2015**, *113* (2), 184−215.
(49) Zhang, J.; P, Z.; Z, R.; H, X.; Z, X.; T, Z.; Zhang, Y.; W, Y.; L, W. *G. Qbics - Quantum Biology, Informatics and Chemistry Server*; Shenzhen Bay Laboratory: Shenzhen, China, 2023.
(50) Marcus, R. A. Electron Transfer Reactions in Chemistry. Theory and Experiment. *Rev. Mod. Phys.* **1993**, *65* (3), 599−610.
(51) Marcus, R. A. On the Theory of Electron-Transfer Reactions. VI. Unified Treatment for Homogeneous and Electrode Reactions. *J. Chem. Phys.* **1965**, *43* (2), 679−701.
(52) Samanta, P. K.; Kim, D.; Coropceanu, V.; Brédas, J.-L. Up-Conversion Intersystem Crossing Rates in Organic Emitters for

https://doi.org/10.1021/acs.jpclett.6c01031
J. Phys. Chem. Lett. 2026, 17, 6233−6244

Thermally Activated Delayed Fluorescence: Impact of the Nature of Singlet vs Triplet Excited States. *J. Am. Chem. Soc.* **2017**, *139* (11), 4042−4051.

(53) Gao, X.; Bai, S.; Fazzi, D.; Niehaus, T.; Barbatti, M.; Thiel, W. Evaluation of Spin-Orbit Couplings with Linear-Response Time-Dependent Density Functional Methods. *J. Chem. Theory Comput.* **2017**, *13* (2), 515−524.

https://doi.org/10.1021/acs.jpclett.6c01031
J. Phys. Chem. Lett. 2026, 17, 6233−6244